Received: 8 November 2018 | Revised: 15 January 2019 | Accepted: 16 January 2019

DOI: 10.1002/dvg.23283

genesis WILEY

TECHNOLOGY REPORT

Efficient GFP-labeling and analysis of spermatogenic cells using the IRG transgene and flow cytometry

Leah L. Zagore | Cydni C. Akesson | Donny D. Licatalosi

Center for RNA Science and Therapeutics, Case Western Reserve University, Cleveland, Ohio

Correspondence
Donny D. Licatalosi, Center for RNA Science and Therapeutics, Case Western Reserve University, Cleveland, OH, 44106, USA.
Email: ddl33@case.edu

Funding information
National Institutes of Health, Grant/Award Numbers: R01 GM107331, T32 GM08056; NIH, Grant/Award Numbers: R01 GM107331, T32 GM08056

Summary

Spermatogenesis is a highly ordered developmental program that produces haploid male germ cells. The study of male germ cell development in the mouse has provided unique perspectives into the molecular mechanisms that control cell development and differentiation in mammals, including tissue-specific gene regulatory programs. An intrinsic challenge in spermatogenesis research is the heterogeneity of germ and somatic cell types present in the testis. Techniques to separate and isolate distinct mouse spermatogenic cell types have great potential to shed light on molecular mechanisms controlling mammalian cell development, while also providing new insights into cellular events important for human reproductive health. Here, we detail a versatile strategy that combines Cre-lox technology to fluorescently label germ cells, with flow cytometry to discriminate and isolate germ cells in different stages of development for cellular and molecular analyses.

KEYWORDS

Cre-lox technology, fluorescence activated cell sorting, spermatogenesis

1 | INTRODUCTION

Mouse spermatogenesis is a powerful model system that has provided important insights into molecular mechanisms balancing cell proliferation, differentiation, and apoptosis; DNA repair and recombination; cell–cell communication; adhesion; and stage-specific transcriptional and post-transcriptional gene regulation (Licatalosi, 2016; Lie, Mruk, Lee, & Cheng, 2010; Song & Wilkinson, 2014; Youds & Boulton, 2011). Continued study of spermatogenic cells has the promise to reveal many key aspects of cell biology, infertility, and testicular cancer (Lin & Matzuk, 2014).

In seminiferous tubules of the postnatal testis, spermatogenesis can be divided into three stages and cell types: mitosis (spermatogonia), meiosis (spermatocytes), and post-meiotic differentiation (spermatids). As germ cells transit through these stages, they interact extensively with Sertoli cells–somatic cells that provide essential nutritional and structural support (Griswold, 1998). During the mitotic phase, spermatogonial stem cells differentiate and progress through a series of divisions with incomplete cytokinesis to generate chains of A2, A3, A4, Intermediate, and type B spermatogonia. Around postnatal day 9 (p9), spermatogonia undergo a final mitotic division to yield primary spermatocytes that enter meiosis (De Rooij & Griswold, 2012; Griswold, 2016). During meiosis, a single round of DNA replication is followed by homologous recombination and two successive cell divisions to produce genetically distinct, haploid round spermatids. Thereafter, spermatids undergo a complex differentiation program to produce spermatozoa. This process (spermiogenesis) involves vast morphological and cytological changes including nuclear repackaging and compaction, cell elongation, flagella development, organelle redistribution, and shedding of a large proportion of the cytoplasm in the form of a cytoplasmic droplet that is engulfed by Sertoli cells. Upon completion of spermiogenesis, germ-Sertoli cell contacts are severed to release spermatozoa into the tubule lumen (Upadhyay, Kumar, Ganeshan, & Balasinor, 2012).

Germ cell development in mice and humans are broadly comparable. As a result, mice are the most commonly used animal genetic model for the study of mammalian reproduction (Jamsai & O'Bryan, 2011). The study of mouse spermiogenesis has been particularly valuable for understanding defects associated with human infertility such as globozoospermia (round-headed spermatozoa) and flagellum abnormalities (Escalier, 2006; Yan, 2009).

Several methods exist to isolate specific germ cell populations—a common prerequisite to investigate cell type-specific regulatory programs in heterogeneous tissue (Meistrich, 1977). Approaches such as STA-PUT, which requires expertise in the morphological identification of germ cells, take advantage of differences in cell size and sedimentation velocity to separate enriched populations of germ cells with high yields (Bryant, Meyer-Ficca, Dang, Berger, & Meyer, 2013). Immunomagnetic isolation can provide highly pure, viable cell populations; however, the number of specific cell types that can be collected is limited (Van der Wee, Johnson, Dirami, Dym, & Hofmann, 2001).

Separation and simultaneous collection of multiple cell populations can be achieved using Hoechst-based flow cytometry approaches (Bastos et al., 2005; Gaysinskaya, Soh, van der Heijden, & Bortvin, 2014). Testicular cell suspensions are stained with the DNA-binding dye bis-benzamide Hoechst 33342 (Ho) followed by fluorescence activated cell sorting (FACS) to discriminate cells based on DNA content and chromosome structure. The latter is possible due to a chromatic shift in Ho emission (from red to blue) as the concentration of DNA-bound Ho increases (Petersen, Ibrahim, Diercks, & van den Engh, 2004). This allows further discrimination of subpopulations of germ cells with the same DNA content such as primary spermatocytes in different steps of meiotic I prophase, and spermatogonia from secondary spermatocytes (both diploid). Although emission spectra of diploid germ cells and somatic testis cells overlap, we have demonstrated that this barrier can be overcome by combining Ho staining with germ cell-specific GFP-labeling (discussed below).

Cre-lox tools have revolutionized cell and developmental biology research. The general approach uses Cre recombinase from bacteriophage P1 to direct site-specific recombination at short sequences (LoxP elements) present in a target gene (Sauer & Henderson, 1988). Using inducible or tissue-restricted promoters, Cre expression can be controlled in a temporal and cell-type specific manner. We previously used Cre-lox to label germ cells with green fluorescent protein (GFP) combined with Ho staining and FACS to quantify spermatogenic defects in 9-week-old mice with germ cell-specific ablation of *Ptbp2* (Zagore et al., 2015). This approach utilizes the Stra8-iCre driver (Sadate-Ngatchou, Payne, Dearth, & Braun, 2008) and the IRG transgene (a LoxP-containing dual fluorescence reporter that switches expression from red to green fluorescent protein after Cre-recombination) (De Gasperi et al., 2008). We also showed that combining these transgenes allows efficient labeling and collection of limiting numbers of spermatogonia present in p6 testes of *Dazl* knockout mice for transcriptome-profiling (Zagore et al., 2018). Although these prior studies highlight the power of GFP-labeling and FACS to quantify and isolate adult and early postnatal germ cells, respectively, a direct comparative analysis of GFP expression in different spermatogenic cell types has not been performed. Furthermore, the usefulness of the IRG transgene as a reagent to study embryonic and perinatal stages of germ cell development was not investigated.

In this report, we further assessed the utility of Cre-lox GFP-labeling of germ cells using the IRG reporter as a tool for spermatogenesis research. Following cells in the first wave of spermatogenesis, we show that GFP is present in all germ cell stages. Furthermore, we show GFP intensity is markedly different between round and elongating spermatids, and that this difference can be exploited as an additional FACS parameter to quantify and isolate round versus elongating spermatids. We also show that the IRG transgene can be used in combination with the Ddx4-Cre driver to label gonocytes during embryogenesis, providing a means to quantify and collect these cells for molecular analyses. Lastly, we quantitate germ cell restricted IRG recombination using two different Cre-drivers (Stra8-iCre and Ddx4-Cre) and demonstrate high specificity and efficiency of this labeling strategy. Collectively, our findings demonstrate that GFP-labeling of germ cells with the IRG transgene and germ cell-specific Cre drivers as an effective research tool to discriminate, quantify, and collect germ cells from perinatal to adult testes.

2 | RESULTS

2.1 | GFP-labeling mitotic, meiotic, and post-meiotic germ cells with Stra8-iCre and IRG

To assess GFP expression during spermatogenesis, we used FACS to examine Ho-stained cells from Stra8-iCre+ IRG+ seminiferous tubules collected at p23, p35, and p42 (Figure 1). After gating for GFP+ cells, three diagonal bands corresponding to 1C, 2C, and 4C cells are evident, as expected (Zagore et al., 2015). Whereas the 1C band contains a single cluster of GFP+ cells, each of the 2C and 4C cells segregate into sub-clusters with either low or high Ho-red fluorescence emission. The five readily discernible cell clusters correspond to: (1) spermatogonia (2C, mitotic), (2) pre-leptotene/leptotene spermatocytes (4C, meiosis I prophase), (3) pachytene/diplotene spermatocytes (4C, meiosis I prophase), (4) secondary spermatocytes (2C, meiosis II), and (5) spermatids (1C, post-meiotic) (Figure 1a). Consistent with a minority of germ cells having completed meiosis by p23, only 15.7% of the GFP+ cells were in population 5 (haploid spermatids) (Figure 1b,e). In contrast, haploid cells comprised a significantly greater proportion of cells in testes from p42 mice, consistent with completion of the first wave of spermatogenesis at ~p35 (Figure 1c,e). Another significant shift was readily observable in the development of early prophase-I spermatocytes (population 2), which decreased from approximately 25% to less than 8% of GFP+ cells at p42. Importantly, the percentage of GFP+ germ cells in each of the five subgroups in testes collected at different ages are consistent with previous cytological analyses (Bellve et al., 1977; Bellvé, Millette, Bhatnagar, & O'Brien, 1977) (Figure 1b–e). These observations show that GFP is continually present throughout spermatogenesis following recombination of the IRG transgene in spermatogonia. They also indicate that dual fluorescence FACS analysis of Stra8-iCre+, IRG+ cells is an effective strategy to discriminate and quantify subpopulations of germ cells in all stages of postnatal spermatogenesis.

We next used fluorescence microscopy to examine GFP-expression in Stra8-iCre+, IRG+ testes collected at p6, p11, p19, p29, and p35 (Figure 2). At p6, type A spermatogonia are the most advanced germ cells present. By p11, meiotic prophase has initiated, and by p19 germ cells have reached the late pachytene stage. Round and elongating spermatids are readily observable at p29, while p35 marks the completion of the first wave of spermatogenesis. Sections were incubated with antibody to GFP and counterstained with

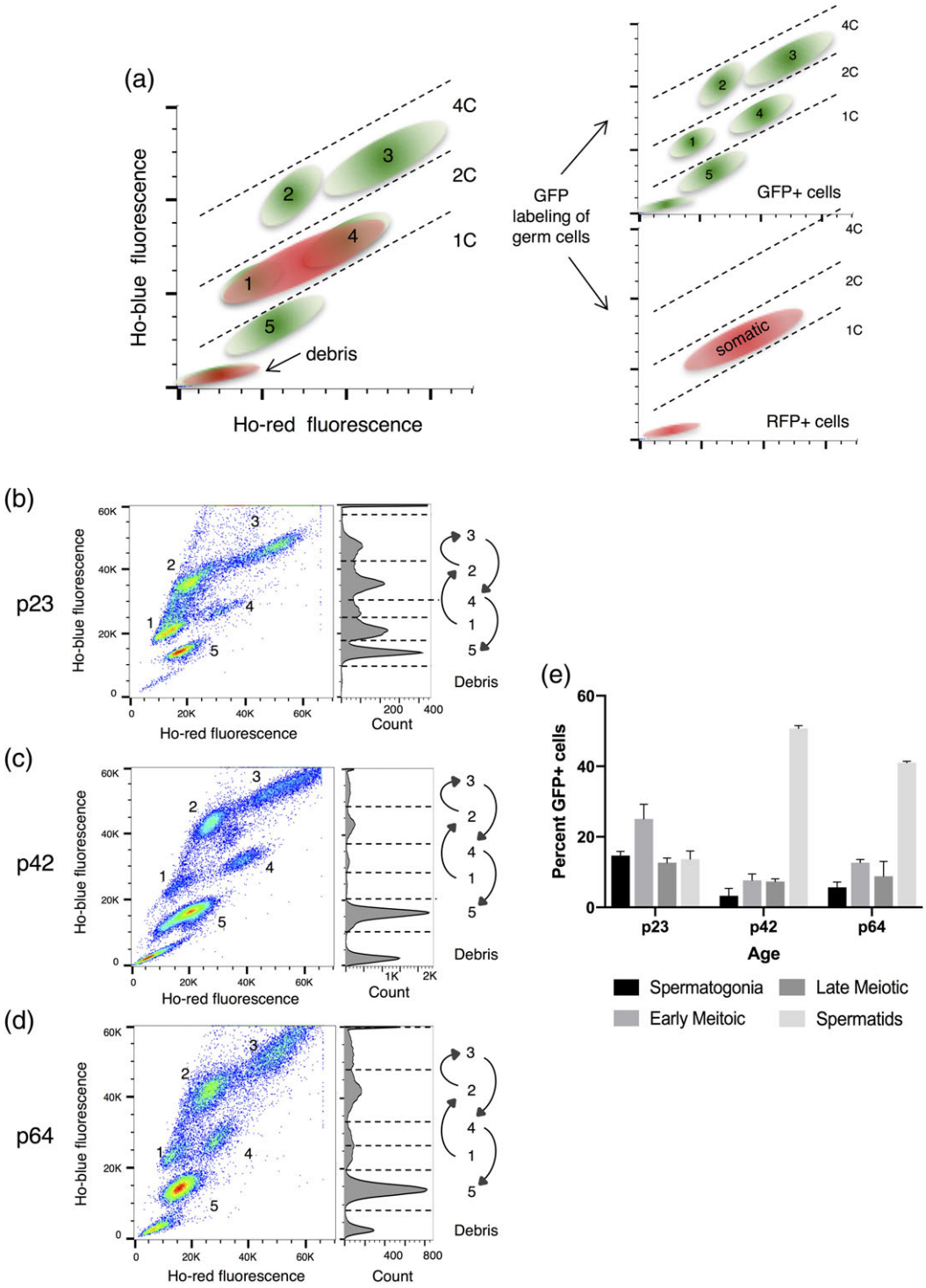

FIGURE 1 Quantitative analysis of the FACS profiles from juvenile and adult testes using the dual fluorescence reporter system. (**a**) Representative image showing a FACS profile from Hoechst 33342 stained adult male testis lysate. Cells cluster into five subpopulations: (1) spermatogonia, (2) early-prophase I spermatocytes, (3) late-prophase I spermatocytes, (4) secondary spermatocytes, and (5) spermatids. Note the resolution of the GFP+ diploid population using fluorescence labeling of germ cells. **(b–d)** Distribution of GFP+, Hoechst 33342-stained cells from C57BL/6J Stra8-iCre+, IRG+ mice at ages p23, p42, and p64, respectively. Histogram to the right shows the distribution of GFP+ cells based on Ho-blue fluorescence values. **e.** Percentage of total GFP positive cells within specific gated germ cell populations. Percentage reported reflects the average percentage of two biological replicates and error bars represent standard deviation

antibody for the germ cell marker DDX4. Consistent with Stra8-iCre expression beginning ~p3 (Sadate-Ngatchou et al., 2008), GFP expressed from the IRG transgene was observed in spermatogonia present in p6 testes. Importantly, GFP was restricted to DDX4+ cells, and greater than 95% of DDX4+ cells were also GFP+ across multiple ages and biological replicates indicating highly efficient and specific labeling using the Stra8-iCre driver (Table 1). The presence of a small subset of DDX4+, GFP− cells is consistent with previous reports that Stra8-iCre is not expressed in a subset of undifferentiated spermatogonia (Sadate-Ngatchou et al., 2008). As expected, the number of GFP

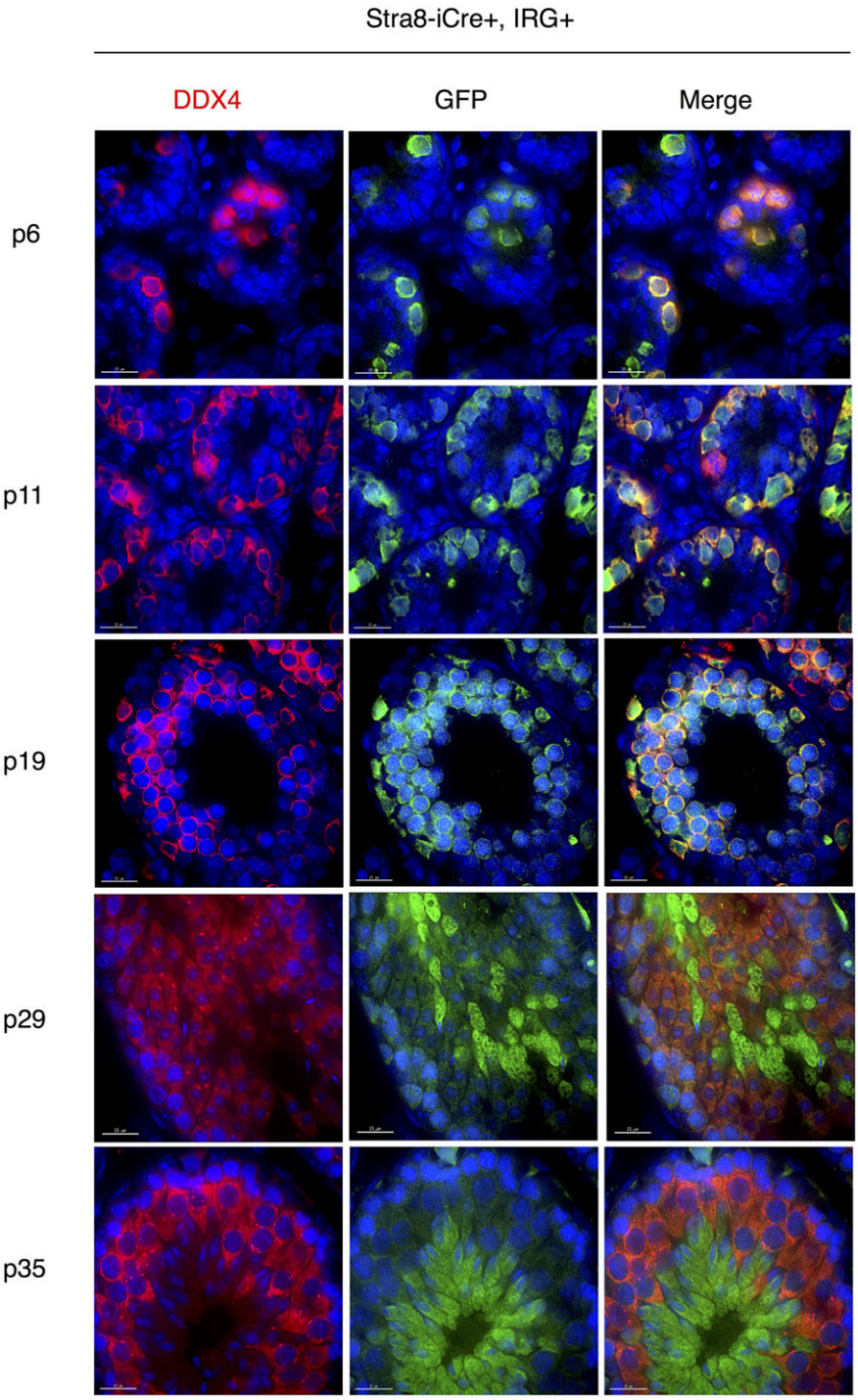

FIGURE 2 Stra8-iCre mediated GFP expression throughout the first wave of spermatogenesis in Stra8-iCre+, IRG+ mice. (**a–e**) Representative images of GFP and Ddx4 expression in seminiferous tubule cross sections at ages p6, p11, p19, p29, and p35 are shown. Note that because of a large dynamic range in GFP expression, GFP intensity is not to scale between different age time points. Scale bars represent 15 μm

+ cells per tubule increased with age as more advanced germ cells accumulated. Therefore, immunofluorescence and FACS confirm that GFP is present in all stages of postnatal germ cell development.

2.2 | Differential GFP levels mark round and elongating spermatids

Immunofluorescence microscopy shows that GFP intensity was comparable in the cytoplasm of spermatogonia, spermatocytes, and round spermatids. Unexpectedly, GFP intensity increased significantly in elongating spermatids. A distinctive process during spermiogenesis is formation of the acrosome—a Golgi and endosome derived vesicle which first appears as a pro-acrosomal granule, then attaches and extends over the nuclear membrane (Berruti, 2016). To determine the precise step when GFP levels increase, we used fluorophore-conjugated PNA to assess acrosome formation and classify spermatids in the 16 defined steps of differentiation (Nakata, Wakayama, Takai, & Iseki, 2015) (Figure 3a–e). Increased GFP intensity was first observed in spermatids at step

TABLE 1 Quantification of Cre-mediated recombination of the IRG transgene using germ cell restricted Cre-drivers

Cre driver	GFP+, DDX4+	GFP−, DDX4+	GFP+, DDX4−	# cells counted	# tubules counted	Ages
Stra8-iCre	97.32%	2.5%	0.180%	560	39	p7, p11, p19
Ddx4-Cre	94%	1.71%	4.27%	117	37	p0

Germ cells were identified as DDX4+ cells and the overlap between GFP+ cells and DDX4+ cells was calculated using two biological replicates. The high number of cells both GFP+ and DDX4+ provide a measure of the efficiency recombination and cell restricted Cre-expression.

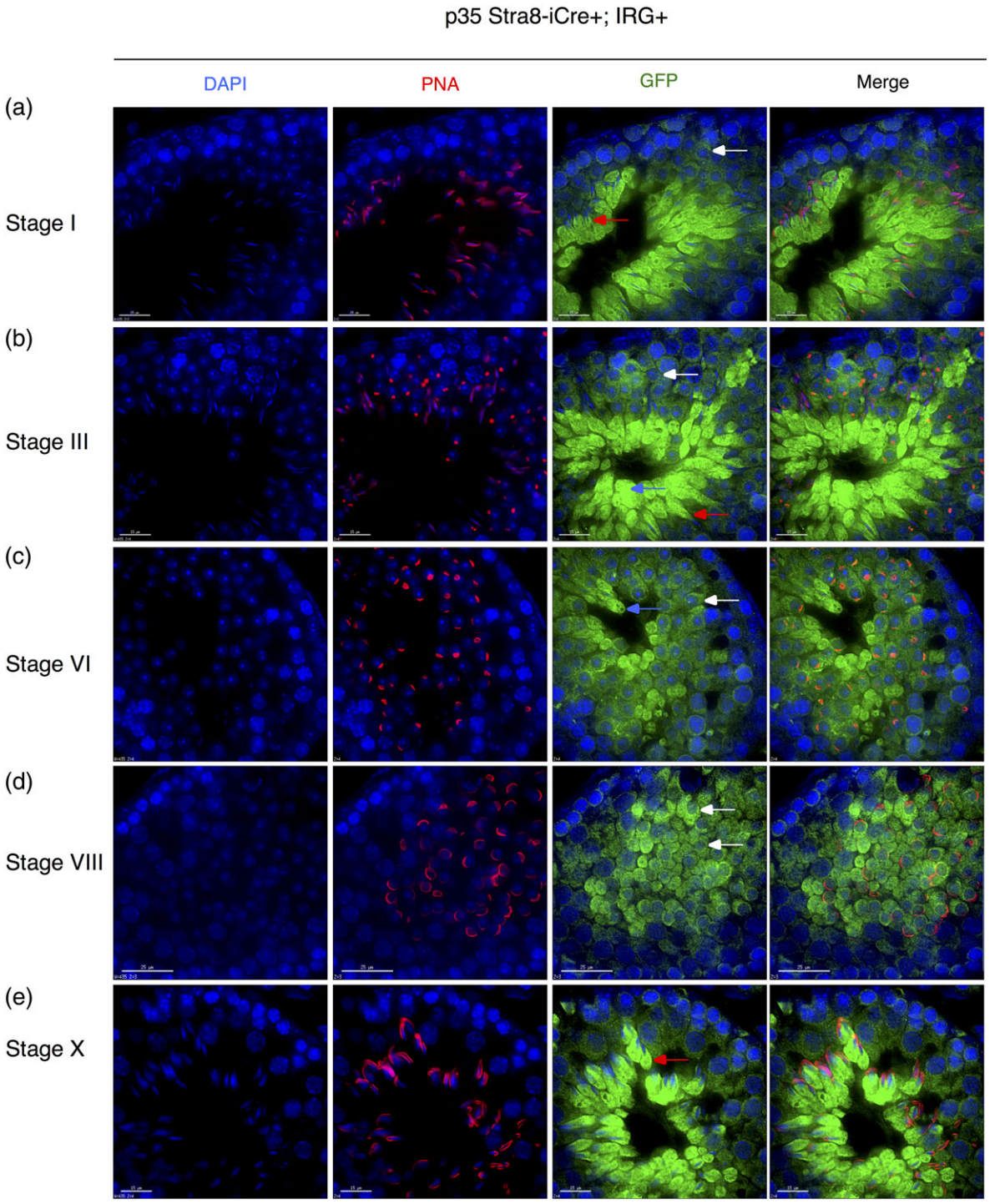

FIGURE 3 Staging of seminiferous epithelial cells to pinpoint the timing of increased GFP expression. (**a–e**) Cross-sections from p35 Stra8-iCre+, IRG+ mouse testes were stained for GFP and peanut agglutinin (PNA) was used to assess acrosomal status. Representative images of spermatogenic stages I, III, VI, VIII, and X are shown. (**a,b**) In spermatogenic stages with multiple populations of spermatids, distinct differences in GFP expression can be observed between round spermatids (white arrows—Spermatid differentiation steps 1–8) and elongating spermatids (red arrows—Spermatid differentiation steps 9–16), with higher GFP signal in the latter. (**b,c**) Blue arrows denote cytoplasmic droplets of step 15–16 spermatids, as they contain no nucleus and high levels of GFP protein. **d.** The subtle difference in GFP expression first begins when round spermatids progress to step 8 (compare white arrows). Scale bars represent 15 μm

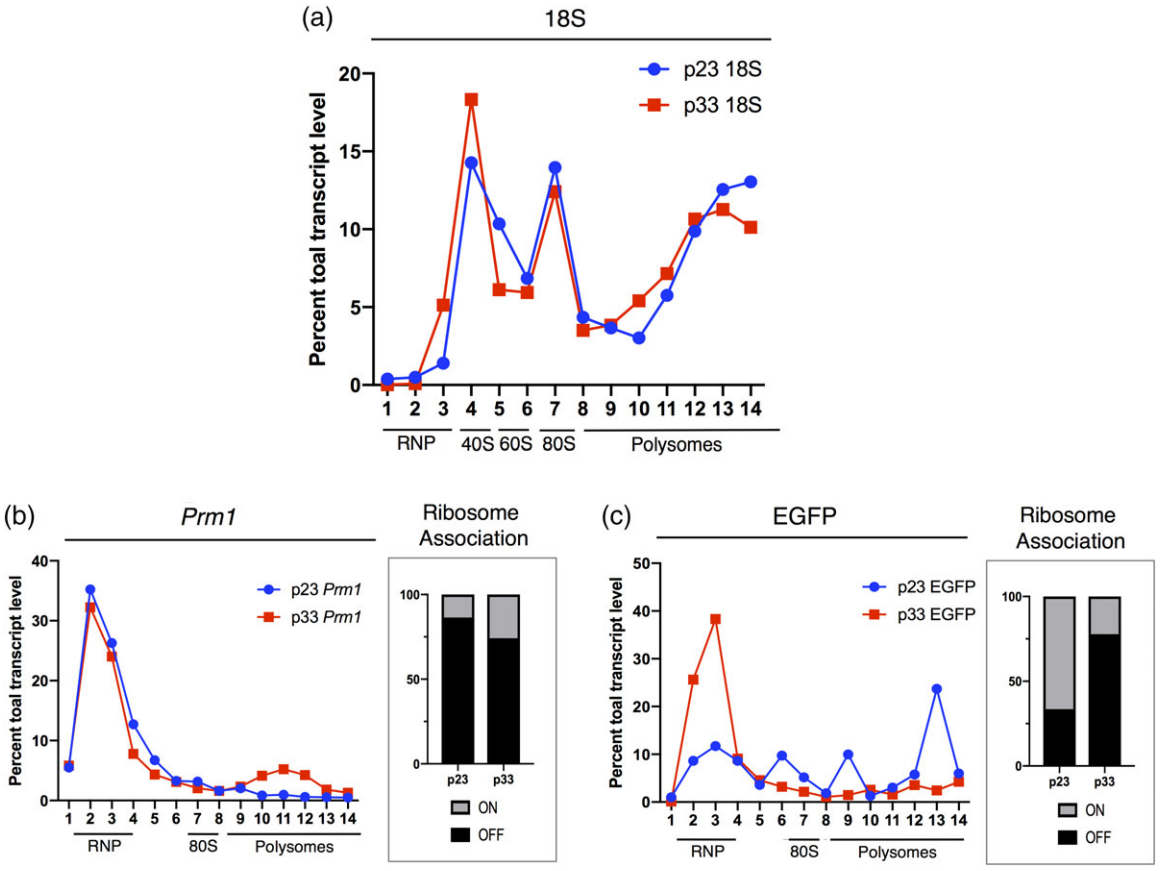

FIGURE 4 Polysome association of GFP transcripts in round and elongating spermatids. (**a**) Distribution of 18S ribosomal RNA (determined by RT-PCR) across a 10–45% sucrose gradient from p23 and p33 mouse testes was used to identify RNP, 40S, 60S, 80S, and polysome-associated fractions. (**b**) Distribution of *Prm1* transcripts across sucrose gradient from p23 Stra8-iCre+, IRG+ mouse testes. Right panel shows overall ribosome association of Prm1 at p23 and p33 age males. (**c**) Distribution of EGFP transcripts across a 10–45% sucrose gradient from Stra8-iCre+, IRG+ mouse testes. Right panel shows overall ribosome association of EGFP mRNA at p23 and p33 age males. "OFF" ribosome was calculated as the sum of total transcripts from fractions 1–5. "ON" ribosome was calculated as the sum of total transcripts from fractions 6–14. Percentage total transcript level reported is the average of two technical replicates

8 (Figure 3d), when the acrosome has spread over approximately one-third of the nucleus and some round spermatids have oriented toward the basal membrane. Thereafter, GFP intensity continually increased and by step 10 elongating spermatids showed a marked difference compared with pachytene spermatocytes (Figure 3e).

During spermatid differentiation, most mRNAs assemble into translationally repressed ribonucleoprotein complexes (RNPs) in a sequence-independent manner (Schmidt, Hanson, & Capecchi, 1999). Only select mRNAs are translated in elongating spermatids. Notably, *Prm1* mRNA is made in round spermatids, maintained in a translationally repressed state, then activated for translation in elongating spermatids (Lee, Haugen, Clegg, & Braun, 1995). Therefore, the observed increase in GFP intensity in elongating spermatids was unexpected, and prompted us to ask if GFP mRNA evades widespread translational repression during spermatid differentiation. To test this possibility, we used sucrose density gradient centrifugation to fractionate mRNAs based on the number of associated ribosomes, followed by qRT-PCR (Figure 4a). As expected (Kleene, 1989), *Prm1* mRNA sedimented in the RNP fraction in lysates from p23 testes (where the most advanced germ cells present are round spermatids), and increased in polyribosome-containing fractions in lysates from p33 testes (which contain elongating spermatids) (Figure 4b). In contrast, GFP mRNA had decreased association with polyribosomes in p33 compared with p23 lysates (from 66 to 22%), indicating decreased translation of GFP protein. Therefore, the increase in GFP intensity is likely due to redistribution and concentration of pre-existing GFP in the cytoplasm of condensing spermatids, rather than increased translation of GFP mRNA.

Since the fluorescence emission spectra of Ho-stained spermatids yields a single cluster of cells (Figure 1), we asked if the differences in GFP intensity observed in round and elongating spermatids by immunofluorescence could be exploited as an additional FACS parameter to separate these subpopulations of cells. We re-examined FACS profiles from Stra8-iCre+, IRG+ testes collected from mature and p23 mice, where the majority of spermatids in the latter have not yet progressed to the elongation steps of differentiation (Figure 5). Consistent with immunofluorescence microscopy, spermatids from p23 contained a single population of GFP+ cells (Figure 5a), while spermatids from older mice separated contained a second population of higher GFP-intensity (Figure 5b,c). These observations indicate that differential GFP levels in round and elongating spermatids can be used a parameter to quantify and collect post-meiotic germ cells for downstream cytological and molecular analyses.

2.3 | Characterization of GFP expression patterns in Ddx4-Cre driver mice

The results described above highlight the utility of the IRG and Stra8-iCre transgenes to GFP-label postnatal germ cells. To expand the applicability of this general approach and GFP label germ cells during embryogenesis (gonocytes), IRG+ mice were bred with mice containing the Ddx4-Cre transgene, which expresses Cre recombinase around E15.5 (Gallardo, Shirley, John, & Castrillon, 2007). Indeed, p0 gonocytes in Ddx4-Cre+, IRG+ males showed strong, cytoplasmic GFP staining (Figure 6). Notably, the majority of GFP expression at p0 and p6 was restricted to germ cells (94%), indicating efficient recombination and minimal ectopic Cre expression (Table 1). These observations confirm expression of the IRG transgene and GFP-labeling in gonocytes, thus providing a means to identify and collect gonocytes from perinatal mice.

2.4 | Discussion

Cell-type specific DNA recombination using Cre-lox technology is a powerful approach to study distinct cell types in tissues with high cellular heterogeneity. We previously took advantage of the Stra8-iCre and IRG transgenes to examine germ cells in adult and early postnatal testes (Zagore et al., 2015; Zagore et al., 2018). Here we further characterized GFP expression during spermatogenesis in Stra8-iCre+ and IRG+ mice to assess the utility of this approach as a general tool for spermatogenesis research. Following germ cell development during the first wave of spermatogenesis, both immunofluorescence microscopy and FACS confirm that GFP is present in all major stages of postnatal development in Stra8-iCre+ and IRG+ testes. Importantly, FACS analysis of Ho-stained GFP+ cells recapitulates known variations in germ cell subpopulations that occur during the first wave of spermatogenesis. These observations illustrate the utility of Ho staining and FACS analysis of IRG mice as a quantitative tool to examine germ cell progression through different stages of development.

While Cre-lox recombination approaches have been implemented in countless studies, expression of Cre does not always follow the expected expression pattern dictated by a given promoter (Smith, 2011). Furthermore, concerns arise as many publications report complications, such as unexpected Cre expression, variable Cre recombination efficiency, and potential toxicity (Eckardt et al., 2004; Matthaei, 2007; Schmidt-Supprian & Rajewsky, 2007). Both Stra8-iCre and Ddx4-Cre drivers performed well in terms of recombination efficiency and cell-type specific recombination of the IRG transgene. However, GFP+ DDX4– cells were more prevalent using the Ddx4-Cre driver as compared with Stra8-iCre driver (4.27 vs. 0.18%). Consequently, if embryonic or perinatal labeling is not required for subsequent analysis, Stra8-iCre may prove a better choice for germ cell restricted Cre recombinase expression. These Cre-drivers could be replaced with other temporally regulated drivers and coupled with FACS; however, further characterization is necessary to assess ectopic Cre expression and unanticipated effects.

The fortuitous observation that GFP intensity differs considerably between round and elongating spermatids provides a simple means to readily separate these two populations of haploid cells by FACS. Importantly, since spermatids are the only haploid cells in the testis, a chromatic shift in Ho fluorescence emission is not required to distinguish GFP+ spermatids from other germ or somatic cell types. As a result, the general strategy described here to distinguish round and elongating spermatids should be compatible with a range of DNA binding dyes and flow cytometers. Therefore, we anticipate that FACS-based discrimination of round and elongating GFP+ spermatids may be a broadly applicable strategy that will benefit researchers studying different aspects of reproductive biology. This includes, but is not limited to, studies of chromatin remodeling and compaction; post-transcriptional gene regulation; and flagellum development—all of which are critical to produce fertile spermatozoa.

3 | MATERIALS AND METHODS

Antibodies		
Rabbit monoclonal anti-GFP	Abcam	Cat#ab183734; RRID: AB_2732027
Mouse monoclonal anti-Ddx4	Abcam	Cat#ab27591; RRID: AB_11139638
Goat anti-mouse IgG (H + L) Alexa Fluor-488 conjugate	Thermo Fisher	Cat#A11017; RRID: AB_143160
Cy3 donkey polyclonal anti-rabbit	Jackson Immuno Research Labs	Cat#711-165-152; RRID: AB_2307443
Lectin PNA, Alexa Fluor-488 conjugate	ThermoFisher	Cat#L21409; RRID: AB_2315178
Reagents		
Fluoromount G	Southern Biotech	Cat#0100-01
Collagenase type I	Worthington Biochemical	Cat#LS004216
Trypsin	Worthington Biochemical	Cat# LS003707
Fetal bovine serum	ThermoFisher	Cat#16140063
bisBenzimide H 33342 trihydrochloride	Sigma-Aldrich	Cat#B2261
Emetine	Sigma-Aldrich	Cat#E2375
Recombinant RNasin	Promega	Cat#N2511
RiboZol RNA extraction reagent	VWR	Cat#97064-950
Turbo DNA free kit	ThermoFisher	Cat#AM1907
Superscript III reverse transcriptase	ThermoFisher	Cat#18080-044
FastStart universal SYBR green master (Rox)	Sigma-Aldrich	Cat#4913850001
TaqMan gene expression assay	ThermoFisher	Cat#Mm04277571_s1

3.1 | Animals and tissue collection

Mice bearing the Stra8-iCre transgene (Tg[Stra8-icre]1Reb/J0, stock No: 008208), IRG transgene (B6;C3-Tg[CAG-DsRed,-EGFP]5Gae/J, stock No: 008605), and Vasa-Cre transgene (FVB-Tg[Ddx4-cre]

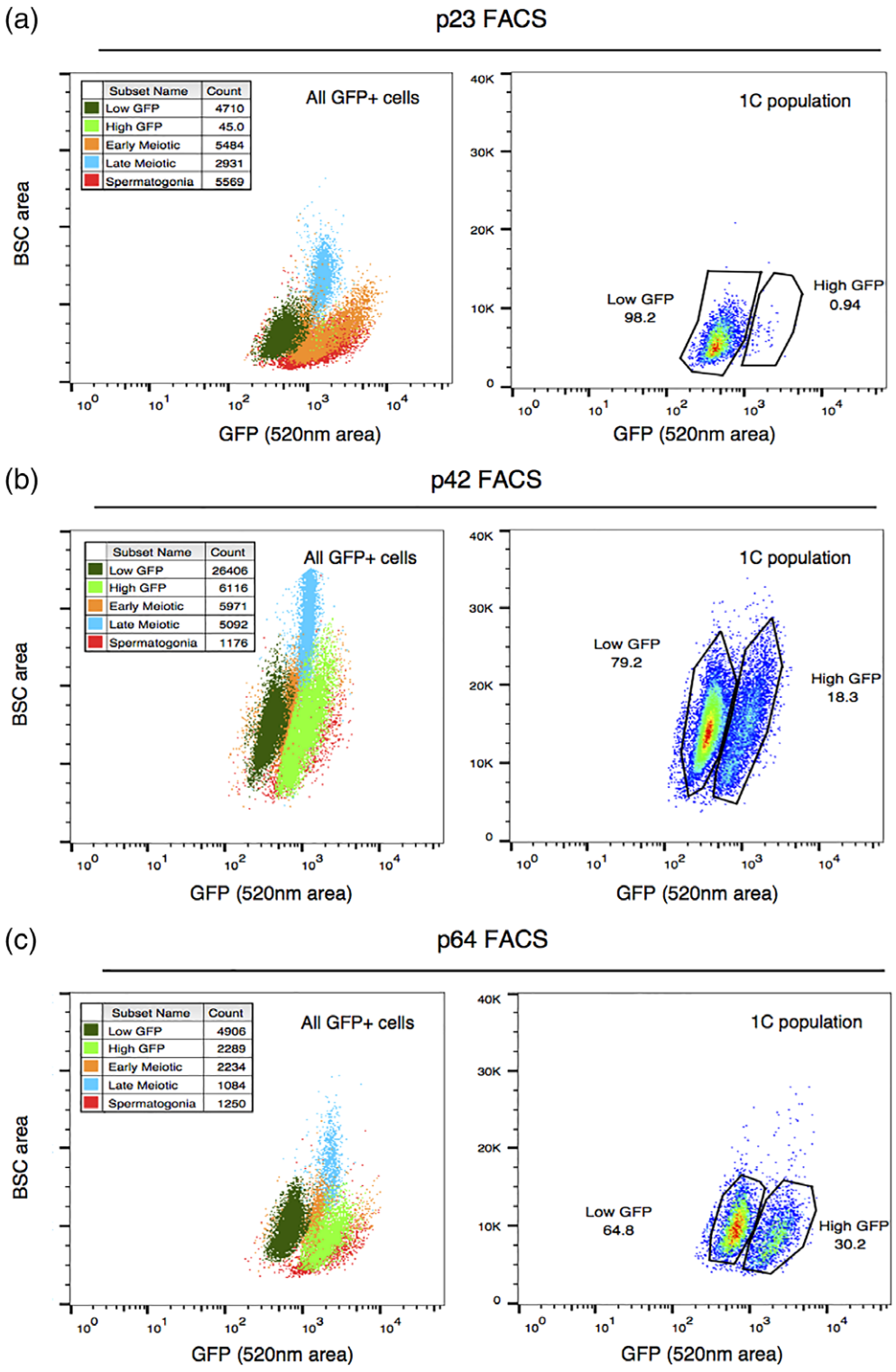

FIGURE 5 Analysis of GFP intensity in Hoechst 33342-stained GFP+ spermatids (**a–c**). The left panel shows GFP intensity of all 5 subpopulations of GFP+ germ cells, dark green: Round spermatids, light green: Elongating spermatids, orange: Early meiotic spermatocytes, blue: Late meiotic spermatocytes, red: Spermatogonia in p23, p42, and p64 Stra8-iCre+, IRG+ mice. For all FACS profiles, the y-axis shows backscatter (BSC area) and the x-axis reports GFP signal (GFP 520 nm area). GFP intensity of spermatid populations (1C population) from Figure 1 (b–d, group 5) was assessed in the right panel. The right panel also reports the quantification of two readily identifiable clusters categorized as "low GFP" or "high GFP," representing round spermatids and elongating spermatids, respectively. Note the absence of elongating spermatids (high GFP) at p23

1DCas/J, stock No: 006954) were purchased from The Jackson Laboratory. C57BL/6J Stra8-iCre++ males were crossed with C57BL/6J IRG+ females to generate C57BL/6J Stra8-iCre+, IRG+ offspring. FVB Vasa-Cre++ males were crossed with C57BL/6J IRG+ females to generate 50:50 FVB:C57BL/6J Vasa-Cre+, IRG+ animals. Mice were sacrificed by isoflurane inhalation followed by cervical dislocation or decapitation. Day of birth was considered p0. All animal procedures were approved by the Institutional Animal Care and Use Committee at CWRU.

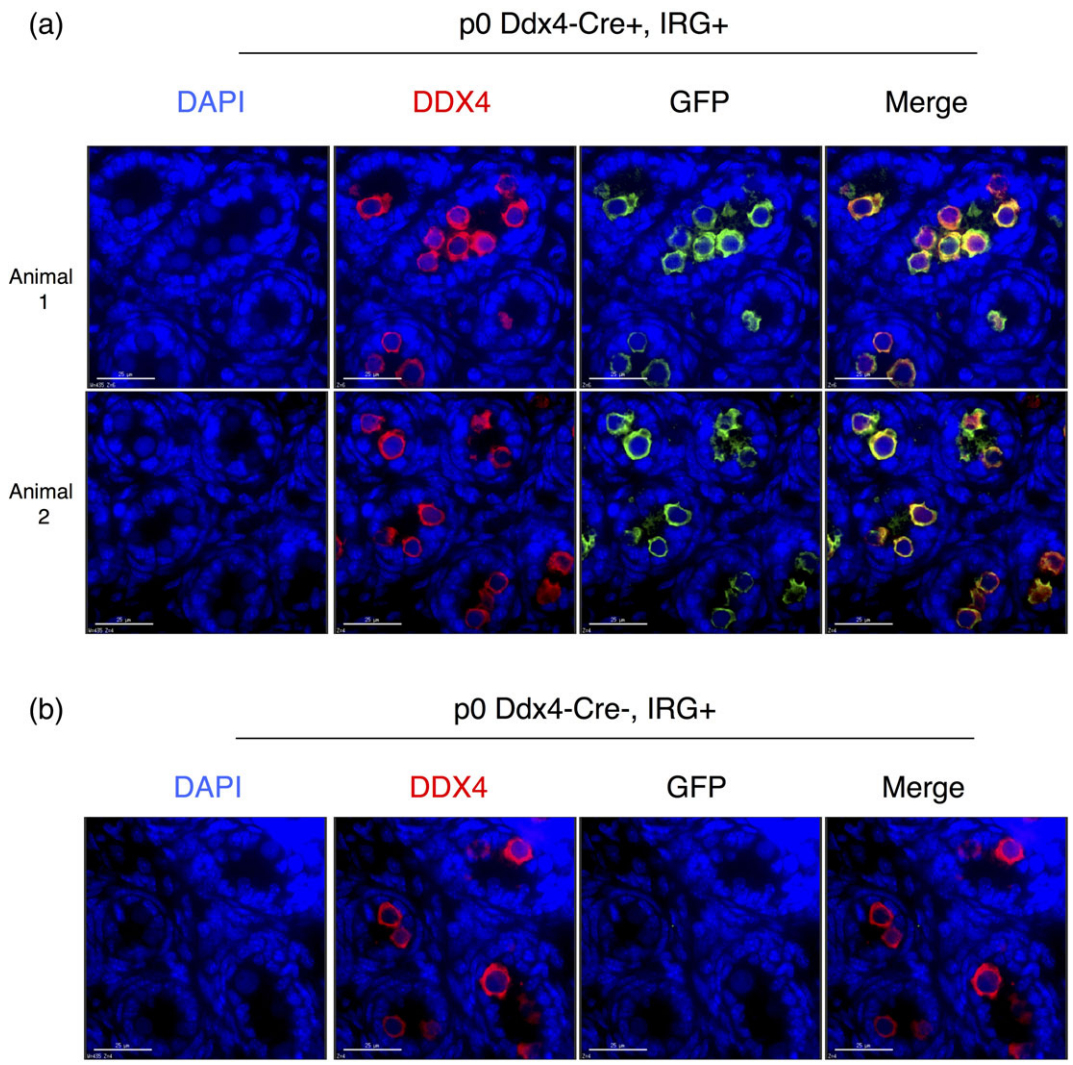

FIGURE 6 Ddx4-Cre mediated GFP expression in p0 Ddx4-Cre+, IRG+ mice. **(a)** Representative images of GFP and DDX4 expression in seminiferous tubule cross-sections at age p0 from two biological replicates. **(b)** Negative control showing lack of GFP expression in p0 Ddx4-Cre-, IRG+ mice. Scale bars represent 25 μm

3.2 | Immunofluorescence microscopy

Testes were detunicated in cold Hank's balanced salt solution (1× HBSS) and fixed overnight at 4 °C in 4% paraformaldehyde. Following fixation, tissue was washed with cold 1× phosphate-buffered saline (PBS) and embedded in paraffin by the Histology Core Facility at CWRU. 5-μm sections of embedded tissue were mounted on glass slides and dried overnight at 37 °C. Sections were deparaffinized with three 5-min washes in xylene, followed by two 5-min washes in 100% ethanol. The tissue was rehydrated by performing the following 5-min washes in decreasing ethanol concentrations—95, 70, and 50% ethanol, followed by tap water. Citrate buffer, pH 6.0 was used for antigen retrieval (10 mM sodium citrate, 0.05% Tween 20), at 95 °C for 20 min. Finally, slides were cooled with tap water for 10 min. Tissue was permeabilized for 10 min using 0.25% Triton X-100 in 1× PBS, and rinsed in PBST (0.1% Tween 20 in 1× PBS). Slides were blocked with 1% bovine serum albumin (BSA) in PBST for 1 hr. Next, slides were incubated with 1:500 anti-GFP (Abcam) and 1:500 anti-Ddx4 (Abcam) for 1 hr followed by three 5-min washes in PBST. An additional 1 hr incubation was performed using 1:100 anti-rabbit Cy3 (Jackson ImmunoResearch) and 1:100 anti-mouse Alexa-488 (ThermoFisher) or 1:500 Lectin-PNA Alexa-488 (ThermoFisher). Three 5-min washes in PBST were performed before staining with 0.5 μg/ml DAPI for 5 min and rinsing in 1× PBS. Finally, the tissue was mounted on coverslips with Fluoromount G (Southern Biotech). Images were captured using a Deltavision Deconvolution Microscope.

3.3 | Flow cytometry analysis of seminiferous epithelial cells

Dual fluorescent FACS approach was performed as previously described (Zagore et al., 2015). Briefly, mouse testes were detunicated in cold 1× GBSS (Sigma) and pooled into a 15 ml conical tube containing 3 ml single-cell suspension buffer (1× GBSS, 120 U/ml collagenase type 1 [Worthington Biochemical]) prewarmed to 33 °C. After addition of 10 μl 1 mg/ml DNaseI (in 50% glycerol), tubes were placed horizontally at 33 °C, 120 rpm, for 15 min to promote dissociation of seminiferous tubules. Following incubation, the conical tubes were placed upright for 1 min to allow tubules to settle. The supernatant

containing interstitial cells was removed using a wide mouth pipet and the collagenase digestion was repeated. Settled tubules were resuspended in 2.5 ml prewarmed (33 °C) 1× GBSS containing 120 U/ml collagenase type I, 10 μl 1 mg/ml DNaseI, and 50 μl 50 mg/ml trypsin (Worthington Biochemical). Tubes were inverted gently to mix and placed horizontally at 33 °C for 15 min at 120 rpm. A wide mouth pipet was used to disrupt tubules for 3 min, followed by the addition of 10 μl 1 mg/ml DNaseI, and 30 μl 50 mg/ml trypsin. The tubes were placed horizontally and incubated again at 33 °C for 15 min at 120 rpm. To inactivate trypsin, 400 μl prewarmed (33 °C) filter sterilized fetal bovine serum (ThermoFisher) was added and cells were pelleted for 5 min at 500 rcf. Finally, the dissociated cells were suspended in 3 ml prewarmed (33 °C) 1× HBSS containing 10 μl 1 mg/ml DNaseI. After counting cells on a hemocytometer, 5 μg Hoechst 33342 (in DMSO, Sigma) was added per million cells. A final 33 °C incubation was performed by placing the tubes horizontally for 30 min at 120 rpm in a light shielding container. The single cell suspension was passed through two 40 μm cell strainers prewetted with 1× HBSS followed by the addition of 5 μl propidium iodide (PI) and 10 μl 1 mg/ml DNaseI to the flowthrough. The cell suspensions were kept on ice in the dark until cell analysis and sorting. FACS was performed on a Reflection highly automated parallel sort (HAPS) module (Sony Biotechnology Inc). FACS profiles were created using FlowJo (Version 10).

3.4 | Sucrose gradient polysome analysis

Mouse testes were collected and detunicated in 1× cold HBSS and flash frozen on dry ice. Tissue was lysed in 320 μl lysis buffer (20 mM HEPES, 100 mM NaCl, 3 mM $MgCl_2$, 0.5% Triton X-100, 100 μg/ml emetine) and disrupted using a 1 ml syringe plunger. Lysates were incubated on ice for 5 min after the addition of 4 μl recombinant RNasin (40 units/μl) (Promega). About 200 μl of lysate was loaded onto a 10–45% sucrose gradient and centrifuged for 2 hr at 4 °C at 40,000 rpm in a Sw41Ti rotor. After centrifugation the gradient was fractionated into 16 fractions (1st and 16th fractions discarded) and stored at −80 °C. 25% of each fraction was used for Ribozol (VWR) RNA isolation followed by isopropanol precipitation. Residual DNA was removed using the Turbo DNA-*free* kit (ThermoFisher) according to manufacturer's instruction (routine DNase treatment using 2 U of Turbo DNase for 30 min at 37 °C). qRT-PCR analysis was performed as previously described (Zagore et al., 2015; Zagore et al., 2018) using the following primers: Prm1 F: CGCCGCTCATACACCATAAG, Prm1 R: GGCGAGATGCTCTTGAAGTC, EGFP F: GGTGAACTTCAAGATCCGCC, EGFP R: CTCAGGTGGTTGTCGGG. 18S ribosomal RNA was assessed using a TaqMan Gene Expression Assay designed for mouse Rn18s (ThermoFisher).

ACKNOWLEDGEMENTS

We are grateful to the following Case Western Reserve University core facilities: Virology, Next Generation Sequencing and Imaging Core (IF microscopy), Cytometry and Microscopy (FACS), and Tissue Resources (embedding). This work was supported by funds from the NIH to L.L.Z. (T32 GM08056) and D.D.L. (R01 GM107331).

AUTHOR CONTRIBUTIONS

L.L.Z and D.D.L conceived of and designed the study. L.L.Z performed the experiments. L.L.Z. and C.C.A performed genotyping and collected tissue for embedding. L.L.Z. and D.D.L wrote the manuscript.

CONFLICT OF INTERESTS

The authors declare that they have no conflicts of interests.

ORCID

Donny D. Licatalosi https://orcid.org/0000-0002-2047-6298

REFERENCES

Bastos, H., Lassalle, B., Chicheportiche, A., Riou, L., Testart, J., Allemand, I., & Fouchet, P. (2005). Flow cytometric characterization of viable meiotic and postmeiotic cells by Hoechst 33342 in mouse spermatogenesis. *Cytometry Part A*, *65A*(1), 40–49.

Bellve, A. R., Cavicchia, J. C., Millette, C. F., O'Brien, D. A., Bhatnagar, Y. M., & Dym, M. (1977). Spermatogenic cells of the prepuberal mouse. Isolation and morphological characterization. *Journal of Cell Biology*, *74*(1), 68–85.

Bellvé, A. R., Millette, C. F., Bhatnagar, Y. M., & O'Brien, D. A. (1977). Dissociation of the mouse testis and characterization of isolated spermatogenic cells. *The Journal of Histochemistry and Cytochemistry*, *25*(7), 480–494.

Berruti, G. (2016). To defining an 'origin'-the case for the mammalian acrosome. *Seminars in Cell & Developmental Biology*, *59*, 46–53.

Bryant, J. M., Meyer-Ficca, M. L., Dang, V. M., Berger, S. L., & Meyer, R. G. (2013). Separation of spermatogenic cell types using STA-PUT velocity sedimentation. *Journal of Visualized Experiments*, *80*, 50648.

De Gasperi, R., Rocher, A. B., Sosa, M. A., Wearne, S. L., Perez, G. M., Friedrich, V. L. J., … Elder, G. A. (2008). The IRG mouse: A two-color fluorescent reporter for assessing Cre-mediated recombination and imaging complex cellular relationships in situ. *Genesis*, *46*(6), 308–317.

De Rooij, D. G., & Griswold, M. D. (2012). Questions about spermatogonia posed and answered since 2000. *Journal of Andrology*, *33*(6), 1085–1095.

Eckardt, D., Theis, M., Döring, B., Speidel, D., Willecke, K., & Ott, T. (2004). Spontaneous ectopic recombination in cell-type-specific Cre mice removes loxP-flanked marker cassettes in vivo. *Genesis*, *38*(4), 159–165.

Escalier, D. (2006). Knockout mouse models of sperm flagellum anomalies. *Human Reproduction Update*, *12*(4), 449–461.

Gallardo, T., Shirley, L., John, G. B., & Castrillon, D. H. (2007). Generation of a germ cell-specific mouse transgenic Cre line, vasa-Cre. *Genesis*, *45*(6), 413–417.

Gaysinskaya, V., Soh, I. Y., van der Heijden, G. W., & Bortvin, A. (2014). Optimized flow cytometry isolation of murine spermatocytes. *Cytometry Part A*, *85A*(6), 556–565.

Griswold, M. D. (1998). The central role of Sertoli cells in spermatogenesis. *Seminars in Cell & Developmental Biology*, *9*(4), 411–416.

Griswold, M. D. (2016). Spermatogenesis: The commitment to meiosis. *Physiological Reviews*, *96*(1), 1–17.

Jamsai, D., & O'Bryan, M. K. (2011). Mouse models in male fertility research. *Asian Journal of Andrology*, *13*(1), 139–151.

Kleene, K. C. (1989). Poly(a) shortening accompanies the activation of translation of five mRNAs during spermiogenesis in the mouse. *Development*, *106*(2), 367–373.

Lee, K., Haugen, H. S., Clegg, C. H., & Braun, R. E. (1995). Premature translation of protamine 1 mRNA causes precocious nuclear condensation and arrests spermatid differentiation in mice. *Proceedings of the National Academy of Sciences of the United States of America*, *92*(26), 12451–12455.

Licatalosi, D. D. (2016). Roles of RNA-binding proteins and post-transcriptional regulation in driving male germ cell development in the mouse. *Advances in Experimental Medicine and Biology*, *907*, 123–151.

Lie, P. P., Mruk, D. D., Lee, W. M., & Cheng, C. Y. (2010). Cytoskeletal dynamics and spermatogenesis. *Philosophical Transactions of the Royal Society of London. Series B, Biological Sciences*, *365*(1546), 1581–1592.

Lin, Y. N., & Matzuk, M. M. (2014). Genetics of male fertility. *Methods in Molecular Biology*, *1154*, 25–37.

Matthaei, K. I. (2007). Genetically manipulated mice: A powerful tool with unsuspected caveats. *The Journal of Physiology*, *582*(Pt 2), 481–488.

Meistrich, M. L. (1977). Separation of spermatogenic cells and nuclei from rodent testes. *Methods in Cell Biology*, *15*, 15–54.

Nakata, H., Wakayama, T., Takai, Y., & Iseki, S. (2015). Quantitative analysis of the cellular composition in seminiferous tubules in normal and genetically modified infertile mice. *The Journal of Histochemistry and Cytochemistry*, *63*(2), 99–113.

Petersen, T. W., Ibrahim, S. F., Diercks, A. H., & van den Engh, G. (2004). Chromatic shifts in the fluorescence emitted by murine thymocytes stained with Hoechst 33342. *Cytometry. Part a*, *60*(2), 173–181.

Sadate-Ngatchou, P. I., Payne, C. J., Dearth, A. T., & Braun, R. E. (2008). Cre recombinase activity specific to postnatal, premeiotic male germ cells in transgenic mice. *Genesis*, *46*(12), 738–742.

Sauer, B., & Henderson, N. (1988). Site-specific DNA recombination in mammalian cells by the Cre recombinase of bacteriophage P1. *Proceedings of the National Academy of Sciences of the United States of America*, *85*(14), 5166–5170.

Schmidt, E. E., Hanson, E. S., & Capecchi, M. R. (1999). Sequence-independent assembly of spermatid mRNAs into messenger ribonucleoprotein particles. *Molecular and Cellular Biology*, *19*(5), 3904–3915.

Schmidt-Supprian, M., & Rajewsky, K. (2007). Vagaries of conditional gene targeting. *Nature Immunology*, *8*(7), 665–668.

Smith, L. (2011). Good planning and serendipity: Exploiting the Cre/lox system in the testis. *Reproduction*, *141*(2), 151–161.

Song, H. W., & Wilkinson, M. F. (2014). Transcriptional control of spermatogonial maintenance and differentiation. *Seminars in Cell & Developmental Biology*, *30*, 14–26.

Upadhyay, R. D., Kumar, A. V., Ganeshan, M., & Balasinor, N. H. (2012). Tubulobulbar complex: Cytoskeletal remodeling to release spermatozoa. *Reproductive Biology and Endocrinology*, *10*, 27.

Van der Wee, K. S., Johnson, E. W., Dirami, G., Dym, T. M., & Hofmann, M. C. (2001). Immunomagnetic isolation and long-term culture of mouse type a spermatogonia. *Journal of Andrology*, *22*(4), 696–704.

Yan, W. (2009). Male infertility caused by spermiogenic defects: Lessons from gene knockouts. *Molecular and Cellular Endocrinology*, *306*(1-2), 24–32.

Youds, J. L., & Boulton, S. J. (2011). The choice in meiosis - defining the factors that influence crossover or non-crossover formation. *Journal of Cell Science*, *124*(Pt 4), 501–513.

Zagore, L. L., Grabinski, S. E., Sweet, T. J., Hannigan, M. M., Sramkoski, R. M., Li, Q., & Licatalosi, D. D. (2015). RNA binding protein Ptbp2 is essential for male germ cell development. *Molecular and Cellular Biology*, *35*(23), 4030–4042.

Zagore, L. L., Sweet, T. J., Hannigan, M. M., Weyn-Vanhentenryck, S. M., Jobava, R., Hatzoglou, M., … Licatalosi, D. D. (2018). DAZL regulates germ cell survival through a network of PolyA-proximal mRNA interactions. *Cell Reports*, *25*(5), 1225–1240.

How to cite this article: Zagore LL, Akesson CC, Licatalosi DD. Efficient GFP-labeling and analysis of spermatogenic cells using the IRG transgene and flow cytometry. *genesis*. 2019;57:e23283. https://doi.org/10.1002/dvg.23283